Shock Wave Interactions in Spherical and Perturbed Spherical Geometries *

S. Dutta[a], E. George[a], J. Glimm[a b] J. W. Grove[c], H. Jin[a], T. Lee[a], X. Li[a], D. H. Sharp[c], K. Ye[a], Y. Yu[a], Y. Zhang[a], M. Zhao[a]

[a] Department of Applied Mathematics and Statistics,
State University of New York at Stony Brook,
Stony Brook NY 11794-3600

[b] Center for Data Intensive Computing,
Brookhaven National Laboratory, Upton NY 11973,

[c] Los Alamos National Laboratory Los Alamos, NM

Abstract

The interaction of shock waves with spherical and perturbed spherical layers provides an interesting and important class of problems. We present recent results for these and related planar geometry problems. We address the following issues:

1. The accuracy of different numerical solution methods,
2. The magnitude of numerical solution errors and their causes,
3. The development of the instabilities,
4. Reduced descriptions for chaotic flows.

1. INTRODUCTION

We are concerned with the interaction of shock waves with each other and especially with fluid density discontinuities (boundaries of fluid layers) in planar and spherical geometries and in perturbations of these geometries. The perturbed problems include classical fluid instabilities of steadily accelerated density jumps (the Rayleigh-Taylor or RT instability) and the impulsive or shock accelerated instability (the Richtmyer-Meshkov or RM instability), also for a fluid density jump. These instabilities arise in a number of contexts, including inertial confinement fusion, supernova explosions, supersonic fuel mixing in a scram jet, and the formation of thunderheads in meteorology and of geological salt domes. Because of the wide interest in these phenomena, the subject has an extensive history [1,2].

*Supported in part by the U.S. Department of Energy, including grants DE-AC02-98CH10886, DE-FG02-90ER25084, DE-FG03-98DP00206, and DEFC02-01ER25461, the NSF Grant DMS-0102480, and the Army Research Office Grant DAAD-190110642.

From a numerical point of view, the primary difficulty in this class of problems lies with the contact discontinuity, or density jump. The shock waves can be resolved with about 3 mesh cells; the width of the numerical shock wave does not grow with time. However, the contact discontinuity has a numerical width of 5 cells initially and in many schemes this number grows (for example with the 1/3 power of the number of time steps). Moreover, these fluid interfaces are highly complex. In fact, the flow starts as unstable and shortly becomes chaotic. Thus the under resolved fluid interfaces become the dominant feature of the flow. In addition, there is a nonlinear coupling, in that the dynamics of a overly diffused interface is not the same as a sharply resolved one. This fact is easy to understand, as it is the density contrast which drives the instability growth in the first place. The diffused interface of an under resolved chaotic flow has a significantly reduced density contrast, and thus a lower instability growth rate. Our preferred solution method is to track the fluid discontinuity. It is given independent degrees of freedom, and moves through the computational mesh with its own dynamics, dividing the fluid flow into distinct domains, each containing a single fluid type [3–7].

The gold standard for assessment of errors in numerical solutions is comparison to experiments. In addition, for sufficiently simple problems, accurate solutions can be obtained with fine enough grids and errors can be assessed by comparison. The systematic study of numerical errors, as computed on realistic grids, is not a standard operating procedure for computational fluid dynamics. We go beyond this, in offering a probabilistic model of solution error, suitable for use in uncertainty quantification. Here the goal is to establish uncertainty (e.g. error bars) for a numerically based scientific prediction, including data uncertainty, numerical or physical model uncertainty, and, as addressed here, numerical solution errors and input uncertainty.

Because of the complexity of the chaotic flow we study here, there is an interest in reduced descriptions of the flow. For many purposes, a detailed pointwise description of the chaotic flow is not needed. This is fortunate as the flow is highly unstable and not reproducible. Rather, statistical averages of the flow are important. These, we hope, will be stable, reproducible, and with luck computable directly. The reduced descriptions of the flow thus involve averaged quantities. Averaging of a nonlinear set of equations opens the troublesome issue of closure relations, which have been much discussed in the literature and for which we offer novel solutions.

2. COMPARATIVE ACCURACY OF NUMERICAL METHODS

We studied the relative accuracy of tracked and untracked simulations of spherical implosions and explosions [8–10], computed in a two dimensional (r, z) axisymmetric (cylindrical) geometry. The exact solution came from a one dimensional purely radial computation, performed with high accuracy. The main comparison was between our Front Tracking code, FronTier and a conventional higher order Godunov code based on a TVD scheme, also of our own construction. The problem was initialized with a spherically symmetric contact (density discontinuity) and approaching it either an inward or outward moving shock wave. The problem was carried through the shock-contact interaction, which produces a transmitted shock wave and a reflected wave. The latter may be either a shock or a rarefaction. Of these two waves, one moves outward and one inward until it

reflects off the origin and eventually reshocks the deflected contact interface. The problem was terminated before this reshock event occurred. For comparable accuracy of solutions, we found that the untracked simulation required between 4 and 8 times as fine a mesh in each linear dimension of the computation as was needed for the tracked simulation. The tracked and untracked simulations used almost identical time per computational space time mesh cell, and thus the tracked simulation was between $4^3 = 64$ and $8^3 = 512$ times as efficient for comparable accuracy. Projecting these results to a full 3D simulation, the efficiency of the tracked solution is still larger.

In Fig. 1, we display side by side the density plots of the tracked and untracked solutions, both computed with a 100×100 grid. In Fig. 2 we show the L_1 error as a function of time for 4 grid levels, 100×100 to 800×800 for both tracked and untracked simulations. Note that coarsest grid tracked error is approximately comparable to the finest grid untracked error in this graph, as asserted above.

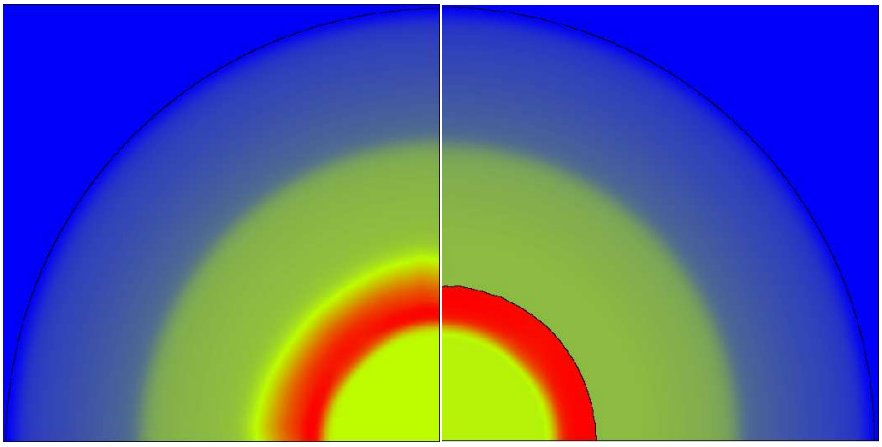

Figure 1. *Density plots for a spherical implosion simulation with an unperturbed interface. The left image shows a contact shocked by implosion shock wave in the untracked case. The right image shows the tracked case at the same time. The grid size is* 100×100.

3. ANALYSIS OF ERRORS

We continue with the study of a spherical implosion. Here we develop a probability model for the errors [11–13]. While the problem is simple enough that this is not a great computational burden, we are interested in more complex problems for which the development of an probability model for numerical errors would be computationally limiting. For this reason, we seek to understand the error and to model its structure. The high point of this analysis is a formula which expresses the error as a sum of individual terms arising from individual wave interactions. These wave interactions are also solved in an isolated setting to construct a probability model for the transmission and creation of errors within each interaction. Our analysis depends on this error analysis for each interaction, treated

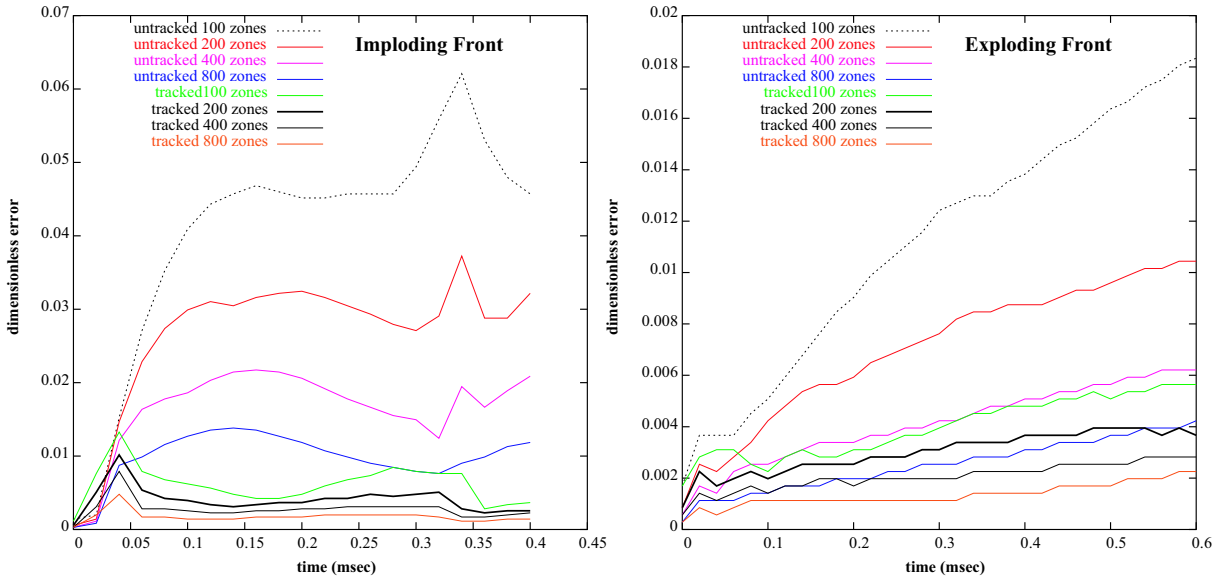

Figure 2. Comparison of tracked and untracked shock implosion (left) and explosion (right) simulations. The L_1 error as a function of time is plotted for 4 grid levels and for both tracked and untracked simulations.

in isolation from the other interactions. Thus the model has as its scientific basis the picture that the errors are either introduced initially (due to uncertain initial conditions) or are created within the simulation at wave interactions only. Between interactions, the errors propagate in a predictable manner. For a planar geometry, the errors are constant between interactions, while for a spherical geometry, the errors grow (if the wave which carries them is moving inward) by a power law in the radius. Similarly outward moving waves and their errors weaken by a power law.

We postulate a 10% uncertainty in the initial conditions, and thereby define an ensemble of simulations and of errors, to be analyzed from a probabilistic point of view. The ensemble is solved on two grid levels, with 100 and 500 cells, in a 1D spherical geometry, and the error is determined by comparison to an ultra fine grid of 2000 cells. The model for the mean total error after the reshock interaction, constructed as outlined above, is generally accurate to one or two digits, with an exception for the coarsest level of simulation and the study of the wave position error. The model, applied to construct the variance of the error, understates the STD by a factor generally between 1.5 and 2, for causes not presently identified. Using the model, the total error is a sum of six terms, each corresponding to a pattern of wave interactions and transmissions. Of these diagrams, two correspond to initial error, following different transmission patterns, and four correspond to errors created within the solution and transmitted to the output of the reshock interaction, where the errors are analyzed. All computations are untracked. The errors are characterized through their mean and standard deviation. By assumption, the initial uncertainty has mean zero. The models for the transmission of error are all linear. This is perhaps surprising in view of the fact that the interactions are highly

nonlinear, but results from the fact that the errors are analogous to perturbations. The linear error transmission model is essentially the first order (linear) variational formula for perturbations of the solution. Errors in this linear model were analyzed previously and generally found to be small. As a result, the mean error associated with the initial error and transmitted to the output of the the reshock interaction is also zero, and only four terms contribute to the mean error. All six terms contribute to the standard deviation. In Fig. 3 we show the six diagrams contributing to the error at the output of the reshock interaction. See also [14].

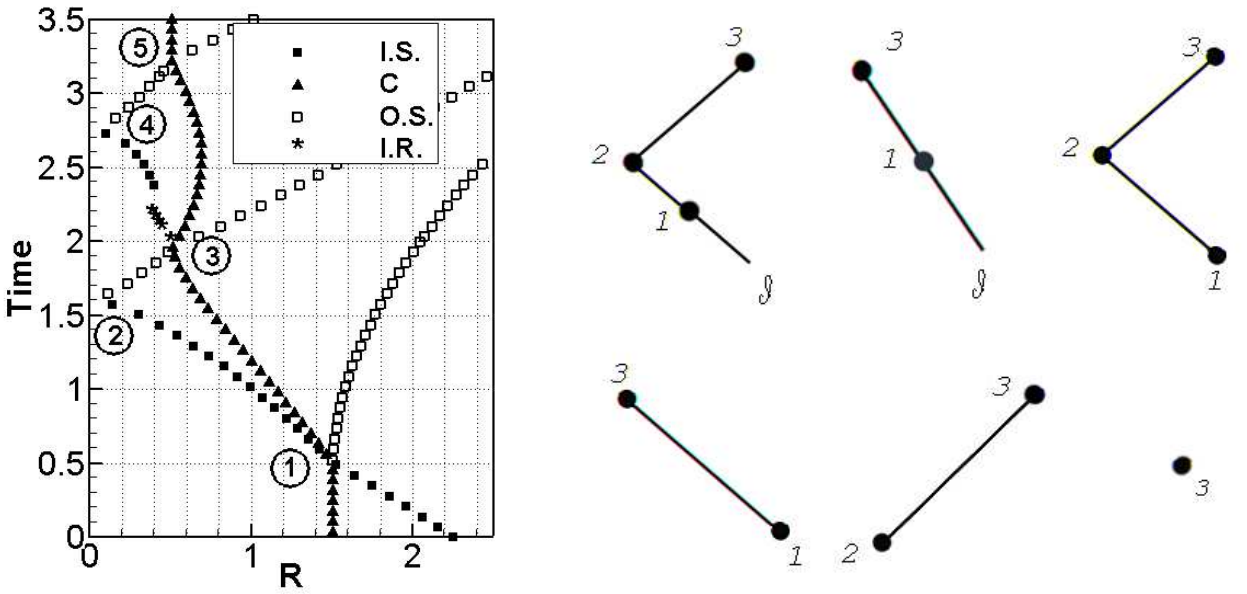

Figure 3. Schematic graphs. Left: the space-time trajectories of the principal waves, as detected by our wave filter program from the untracked solution. Here IS and OS denote inward and outward moving shocks, C is a contact and IR is an inward rarefaction. Right: all six wave diagram contributions to the errors or uncertainty in the output from a single Riemann solution, namely the reshock interaction (numbered 3 in the left frame) of the reflected shock from the wall as it crosses the contact. The numbers labeling the black circles refer to the Riemann interactions contributing to the error. The letter $\mathcal{I}$ in the first two diagrams indicates input uncertainty.

All six terms contribute to the variance and its square root, the standard deviation σ. It is customary to regard $\pm 2\sigma$ as the size of the error bars to be added to the simulation. Additionally, the mean error is subtracted from the simulation value to correct for systematic bias in the coarse grid simulation. In Fig. 4, we plot the relative sizes of the variance for each of the 6 graphs. Note that the two associated with input uncertainty are

hatched and the others are solid gray scales. We see that for a 500 cell grid, the dominant error comes from the initial uncertainty, while for the 100 grid over 75% of the error arises within the numerical simulation.

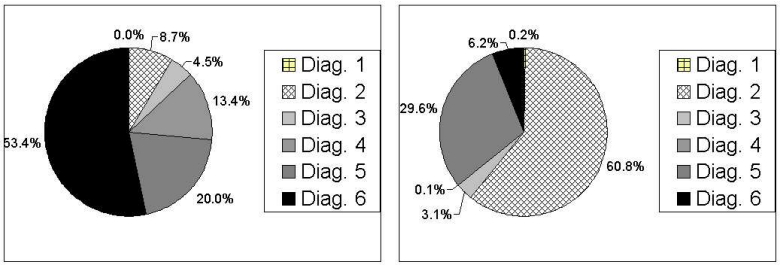

Figure 4. Variance of error or uncertainty associated with each of the six wave diagrams contributing to the post reshock wave strength for the contact wave. The two circle graphs represent 100 and 500 cell simulations, respectively. The two diagrams associated with input uncertainty are shown in hatched gray. Note that these diagrams are dominant for the 500 cell simulation, but that the sum of the created errors are dominant for the 100 cell simulation.

4. INSTABILITY PHENOMENA

We now address the much more difficult question of the perturbed interface problem, with the ensuing instability growth and chaotic flow. Before we can apply the above methods of statistical error analysis, we require a numerical solution procedure which is $\mathcal{O}(1)$ correct. This simply stated and seemingly elementary requirement has proven to be surprisingly difficult for the scientific community. Our present results apply to a planar geometry. After the first correct RM simulation (to achieve agreement with experimental data) by FronTier [15,16], a three way code comparison, with experimental data from laser acceleration and a theoretical model all achieved agreement for a single mode 2D RM instability [17]. This result is very encouraging, but the mesh resolution used to achieve it was not, in view of the desire to compute the much more difficult instabilities in 3D and for fully chaotic (as opposed to single mode) flows. For the related RT chaotic instability in 3D, extensive studies have shown that most simulation codes compute an instability growth rate which is below the experimental value by about a factor of 2, while the FronTier values [18–20] are consistent with the experimental range of values, but on the high side. We have analyzed the tracked and untracked simulations and found a simple explanation of this difference.

Most untracked simulations are performed on an under resolved grid, so that the width of the diffused interface is of the same magnitude as the unstable fingering structures in the flow. As a result, the diffusion is in effect global, and the density contrast is reduced, by about one half, thereby explaining the factor of 2 reduction in the instability

growth rate for the diffusive calculations [19,20]. This explanation is totally quantitative. The diffusive mixing rate leads to a corrected or renormalized density contrast, and a new determination of the mixing rate, in terms of the density contrast as observed in the simulation. This error-corrected mixing rate for the untracked simulations is in agreement with experiment, leading to agreement for all experiments, all simulations, and with theory [21].

While there appears to be growing acceptance of the mass diffusion explanation for the discrepancy between most (untracked) simulations and experiment, we should mention an alternate theory, that the experiments are contaminated by long wave noise, which drives the growth rates higher. This theory requires comparable and experimentally reproducible noise levels in four completely different series of experiments, based on different physical methods of acceleration, but it also has an additional problem. In truth, we believe that both ideas can be fractionally correct and each contributes to the total observed growth rates. But since the quantitative method of mass diffusion error correction yields agreement of simulation with experiment, there seems to be little room for additional correction from experimental long wave length noise. We expect that the noise will play a smaller role, perhaps explaining the differences in growth rates observed among different experiments.

The error correction of the mixing rate based on an observed density contrast was also applied to highly compressible RT mixing. Here the compressibility leads to a stratification of the density field as a function of the vertical dimension (z). The density stratification destroys self similarity of the flow, but the time dependent density contrast interpretation of the mixing rate restores self similarity, so that scaling laws continue to apply to the highly compressible case. With these error-correcting (for diffusion) and stratification-correcting (for compressibility) methods of data analysis, tracked and untracked simulations agree. They display a strong dependence on compressibility, with a doubling or tripling of the mixing rate in comparison to the much studied and measured incompressible values.

The significance of this extended self similar analysis for compressible flows is potentially large, as many interesting flows are highly compressible, and (as we see in the next section) the growth rates of the self similar flows play a large role in the parametrization (closure) of the reduced description simulations.

5. REDUCED DESCRIPTIONS OF CHAOTIC MIXING

Chaotic flows display a wealth of detail which is not reproducible, neither experimentally nor in simulations. Generally speaking, this detail is not relevant, and fortunately, only the statistical averages of the detail are of importance. Thus direct numerical simulation (DNS) of mix, as discussed in the previous section, gives more information than is needed, and information which in detail cannot be reproducible. Since we really want the averages of the DNS simulations, the natural question is to find averaged equations which will compute the averaged quantities directly, without use of the difficult intermediate DNS step.

Averaged equations arise in many areas of science. Generally, when the original equations are nonlinear, or when the coefficients of a linear term are to be averaged, lengthy

discussions of how to formulate the averaged equations ensue. The issue is that nonlinearities do not commute with averaging, so the average of a nonlinear function is not equal to the function evaluated at the average value of its argument. In addition, the phenomena at a physics level are much richer, as the averages depend on the averaging length scale. We wish to average over each phase, and end up with multi-phase flow equations. The nonlinear closure terms will then reflect the forces, etc., exerted between the two phases.

For mix at a molecular level, all the nonlinear closure issues occur in the equation of state, which must describe the pressure and other thermodynamic functions of an atomic mixture of multiple species. In this case all species have common velocities and temperatures. If the mixing is less fine grained, we call the problem chunk mix. The complete first order multiphase averaging of the microphysical equations leads to such a model, in which each species has separate velocities and thermodynamics (pressure and temperature). We have recently found a closure of this type which preserves all requirements of an obvious physical nature: required boundary conditions at the edges of the mixing zone, conservation of species mass, total momentum, total energy and for smooth flows, phase entropy [22]; see also earlier work [23,24] and references cited there. The only parameters to be fixed in this closure are determined by the growth rates for the edges of the mixing zone.

An additional feature of the closure [22] is a coupling between the growth rates of the two edges (bubble and spike, or penetration of light fluid into heavy and the reverse) of the mixing zone. Only one of these growth rates is independent according to this theory. Earlier studies of incompressible flow, both theoretical and based on analysis of experimental data reached the same conclusion [25–28].

Whether the two pressure closure mentioned above (which is hyperbolically stable for time propagation) is used or the more common equal pressure closure (which requires a minimum level of diffusion for stability) is used, the closure contains parameters. The parameters are set to obtain agreement of the overall growth rate with experiment for self similar mixing. Thus extension of self similar mixing to a strongly compressible regime, with modified self similar growth rates, implies a strongly compressible modification of common closure parameterizations.

REFERENCES

1. S. Chandrasekhar. *Hydrodynamic and Hydromagnetic Stability.* Oxford University Press, Oxford, 1961.
2. D. H. Sharp. An overview of Rayleigh-Taylor instability. *Physica D*, 12:3–18, 1984.
3. J. Glimm, J. W. Grove, X.-L. Li, K.-M. Shyue, Q. Zhang, and Y. Zeng. Three dimensional front tracking. *SIAM J. Sci. Comp.*, 19:703–727, 1998.
4. J. Glimm, J. W. Grove, and Y. Zhang. Interface tracking for axisymmetric flows. *SIAM J. SciComp*, 24:208–236, 2002. LANL report No. LA-UR-01-448.
5. J. Glimm, J. W. Grove, Y. Zhang, and S. Dutta. Numerical study of axisymmetric Richtmyer-Meshkov instability and azimuthal effect on spherical mixing. *J. Stat. Physics*, 107:241–260, 2002.
6. J. Glimm, X.-L. Li, and Y.-J. Liu. Conservative front tracking with improved accuracy. *SIAM J. Numerical Analysis*, 41:1926–1947, 2003.

7. J. Glimm, X.-L. Li, Y.-J. Liu, and N. Zhao. Conservative front tracking and level set algorithms. *Proc. National Academy of Sci.*, 98:14198–14201, 2001.
8. S. Dutta, J. Glimm, J. W. Grove, D. H. Sharp, and Y. Zhang. Error comparison in tracked and untracked spherical simulations. *Computers and Mathematics with Applications*, 2003. accepted, University at Stony Brook preprint number AMS-03-10 and LANL report No. LA-UR-03-2920.
9. S. Dutta, J. Glimm, J. W. Grove, D. H. Sharp, and Y. Zhang. A fast algorithm for moving interface problems. In V. Kumar et al., editor, *Computational Science and Its Applications - ICCSA 2003, LNCS 2668*, pages 782–790. Springer-Verlag, Berlin Heidelberg, 2003. LANL report No. LA-UR-02-7895.
10. S. Dutta, J. Glimm, J. W. Grove, D. H. Sharp, and Y. Zhang. Spherical Richtmyer-Meshkov instability for axisymmetric flow. *Mathematics and Computers in Simulations*, 2003. in press; University at Stony Brook preprint number AMS-03-13.
11. B. DeVolder, J. Glimm, J. W. Grove, Y. Kang, Y. Lee, K. Pao, D. H. Sharp, and K. Ye. Uncertainty quantification for multiscale simulations. *Journal of Fluids Engineering*, 124:29–41, 2002. LANL report No. LA-UR-01-4022.
12. J. Glimm, J. W. Grove, Y. Kang, T. Lee, X. Li, D. H. Sharp, Y. Yu, K. Ye, and M. Zhao. Statistical riemann problems and a composition law for errors in numerical solutions of shock physics problems. *SISC (In Press)*, 2003. University at Stony Brook Preprint Number SB-AMS-03-11, Los Alamos National Laboratory number LA-UR-03-2921.
13. J. Glimm, J. W. Grove, Y. Kang, T. Lee, X. Li, D. H. Sharp, Y. Yu, K. Ye, and M. Zhao. Errors in numerical solutions of spherically symmetric shock physics problems. *Contemporary Mathematics*, 2004. (submitted) University at Stony Brook Preprint Number SB-AMS-04-03, Los Alamos National Laboratory number LA-UR-04-0713.
14. T. Lee, Y. Yu, M. Zhao, J. Glimm, X. Li, and K. Ye. Error analysis of composite shock interaction problems. *Conference Proceedings of PMC04*, 2004. (submitted) University at Stony Brook Preprint Number SB-AMS-04-08.
15. R. L. Holmes. *A Numerical Investigation of the Richtmyer-Meshkov Instability Using Front Tracking*. PhD thesis, State Univ. of New York at Stony Brook, 1994.
16. R. L. Holmes, J. W. Grove, and D. H. Sharp. Numerical investigation of Richtmyer-Meshkov instability using front tracking. *J. Fluid Mech.*, 301:51–64, 1995.
17. R. L. Holmes, B. Fryxell, M. Gittings, J. W. Grove, G. Dimonte, M. Schneider, D. H. Sharp, A. Velikovich, R. P. Weaver, and Q. Zhang. Richtmyer-Meshkov instability growth: Experiment, simulation, and theory. *J. Fluid Mech.*, 389:55–79, 1999. LA-UR-97-2606.
18. J. Glimm, J. W. Grove, X. L. Li, W. Oh, and D. H. Sharp. A critical analysis of Rayleigh-Taylor growth rates. *J. Comp. Phys.*, 169:652–677, 2001.
19. E. George, J. Glimm, X. L. Li, A. Marchese, and Z. L. Xu. A comparison of experimental, theoretical, and numerical simulation Rayleigh-Taylor mixing rates. *Proc. National Academy of Sci.*, 99:2587–2592, 2002.
20. E. George and J. Glimm. Self similarity of Rayleigh-Taylor mixing rates. *Phys. Fluids*, 2004. Submitted. Stony Brook University Preprint number SUNYSB-AMS-04-05.
21. B. Cheng, J. Glimm, and D. H. Sharp. A three-dimensional renormalization group

bubble merger model for Rayleigh-Taylor mixing. *Chaos*, 12:267–274, 2002.
22. H. Jin, J. Glimm, and D. H. Sharp. Two-pressure two-phase flow models. *ZAMP*, 2003. Submitted. Stony Brook University Preprint number SUNYSB-AMS-03-16 and Los Alamos National Laboratory LAUR Number LA-UR-03-7279.
23. H. Jin. *The Incompressible Limit of Compressible Multiphase Flow Equations.* PhD thesis, SUNY at Stony Brook, 2001.
24. J. Glimm, H. Jin, M. Laforest, F. Tangerman, and Y. Zhang. A two pressure numerical model of two fluid mixing. *SIAM J. Multiscale Model. Simul.*, 1:458–484, 2003.
25. B. Cheng, J. Glimm, D. Saltz, and D. H. Sharp. Boundary conditions for a two pressure two phase flow model. *Physica D*, 133:84–105, 1999.
26. B. Cheng, J. Glimm, and D. H. Sharp. Density dependence of Rayleigh-Taylor and Richtmyer-Meshkov mixing fronts. *Phys. Lett. A*, 268:366–374, 2000.
27. B. Cheng, J. Glimm, and D. H. Sharp. Dynamical evolution of the Rayleigh-Taylor and Richtmyer-Meshkov mixing fronts. *Phys. Rev. E*, 66:1–7, 2002. Paper No. 036312.
28. B. Cheng, J. Glimm, X. L. Li, and D. H. Sharp. Subgrid models and DNS studies of fluid mixing. In E. Meshkov, Y. Yanilkin, and V. Zhmailo, editors, *Proceedings of the 7th International Conference on the Physics of Compressible Turbulent Mixing, (1999)*, pages 385–390, Sarov, Nizhny Novgorod region, Russia, 2001. RFNC-VNIIEF.